Available online at www.sciencedirect.com

ScienceDirect

Advances in Space Research 72 (2023) 1183–1195

ADVANCES IN SPACE RESEARCH (a COSPAR publication)

www.elsevier.com/locate/asr

Satellite-based electron density background definition at mid-latitudes and comparison with IRI-2016 model under different solar conditions

Dario Sabbagh [a,*], Alessandro Ippolito [a], Dedalo Marchetti [b], Loredana Perrone [a], Angelo De Santis [a], Saioa A. Campuzano [c], Gianfranco Cianchini [a], Alessandro Piscini [a]

[a] *Istituto Nazionale di Geofisica e Vulcanologia, via di Vigna Murata 605, 00143 Rome, Italy*

[b] *College of Instrumentation and Electrical Engineering, Jilin University, West Minzhu Street, 938, 130061, Chaoyang District, Changchun City, Jilin Province, China*

[c] *Department of Earth Physics and Astrophysics, Faculty of Physics, Complutense University of Madrid, Pl. de las Ciencias, 1, 28040 Madrid, Spain*

Received 9 March 2023; received in revised form 10 May 2023; accepted 16 May 2023
Available online 22 May 2023

Abstract

A new method to define a background for the ionospheric electron density (N_e) is proposed, making use of mid-latitude measurements under different solar conditions from the Langmuir Probes onboard CHAMP and three identical Swarm satellites. In particular, CHAMP measurements during the years 2004 and 2009, and Swarm observations during 2016 and 2017 have been considered in the 15°-wide latitudinal belt from 35°N to 50°N, and from 0° to 360° in longitude. CHAMP/Swarm in-situ N_e measurements have been then used to check and compare this new defined background with the one computed directly from IRI-2016 N_e output at satellite altitude. The distributions of the relative deviations between the two backgrounds, and of positive and negative anomalies (i.e., N_e variations from each background greater than 30%) with respect to the geomagnetic activity levels have been evaluated under each investigated condition, namely year/satellite, season, night-time or noon hours. Results of this comparison highlight a general overestimation of N_e from IRI during noon hours, while a better agreement between the two backgrounds is found during night-time. However, an underestimation of IRI with respect to Swarm-derived background is found for 2017 data. Finally, the analysis of 2004 plasma data suggests that the IRI-2016 model can be used as a background during periods characterized by high levels of geomagnetic activity. Due to the difficulties to construct a background for satellite data, the proposed method can be considered an useful tool for analyses of electron density variations at the heights of the satellites in Low Earth Orbits (LEO).

Keywords: Ionosphere; Characterization; Electron density; Background; Anomalies; Satellite data; CHAMP; Swarm

1. Introduction

The ionosphere, i.e., the ionized layer of the uppermost portion of Earth's atmosphere, is an important subject of study relevant to numerous technological applications involving radio signals, like high frequency (HF) radio-communications, over-the-horizon radar techniques, satellite-based positioning and navigation services for military and civil uses. The ionosphere plays a unique role in

* Corresponding author.
E-mail addresses: dario.sabbagh@ingv.it (D. Sabbagh), alessandro.ippolito@ingv.it (A. Ippolito), dedalomarchetti@jlu.edu.cn (D. Marchetti), loredana.perrone@ingv.it (L. Perrone), angelo.desantis@ingv.it (A. De Santis), sacampuzano@ucm.es (S.A. Campuzano), gianfranco.cianchini@ingv.it (G. Cianchini), alessandro.piscini@ingv.it (A. Piscini).

https://doi.org/10.1016/j.asr.2023.05.029
0273-1177/

the terrestrial environment because of its marked coupling with the overlying and underlying regions. Sun-Earth interactions play the leading role in its formation, due to solar photoionization by ultraviolet (UV) and soft x-ray radiation, capable of dislodging an electron from a neutral gas atom or molecule upon collision (Hargreaves et al., 2007; Frank-Kamenetsky and Troshichev, 2012). Free electrons present in the Earth's ionosphere persist for long enough periods before recombining into neutral atoms or molecules, affecting radio wave propagation.

Since the nature of the ionosphere is strongly linked to fluctuations in solar emissions, it is consequently highly variable. Violent solar phenomena can significantly affect the physical state of the near-Earth space up to the Earth magnetosphere and ionosphere, producing relevant Space Weather effects. Adverse Space Weather conditions could cause a degradation of HF communications, narrowing the working frequency band due to negative ionospheric storms so that the International Civil Aviation Organization (ICAO) makes use of four Global Space Weather Centers for Aviation (SWX) to monitor the extreme Space Weather events (Kauristie et al., 2021; Fiori et al., 2022).

It should be stressed that the ionosphere-thermosphere is a single system. During a geomagnetic storm, the energy input at high latitudes affects the upper atmosphere producing changes in thermospheric wind and composition (Prölss, 1991; Fuller-Rowell et al., 1994). Next to the ionospheric variations related to an increase of geomagnetic activity there are ionospheric perturbations which occur under quiet geomagnetic conditions whose magnitude is comparable to moderate storm effects (Perrone et al., 2020).

The characterization of the topside ionosphere, namely the region above the ionospheric electron density (N_e) maximum, is of particular importance for satellite operations and for any application involving signals from satellites, being the environment in which the satellites fly. This is of paramount importance due to the present high-technology civilization of humans whose crucial activities rely on satellite data. Space Weather events can indeed threaten satellite transmissions and instruments, affecting avionics in extreme circumstances, and reducing the useful life of satellites in low Earth orbits (LEO).

This paper is focused on the characterization of the mid-latitude topside N_e perturbations under geomagnetically quiet and perturbed conditions, using in-situ measurements from LEO satellites.

In-situ N_e observations linked with ground-based observations as ionosondes and Incoherent Scatter Radars (ISR) are important to define the morphology of N_e. For this purpose, it is fundamental to have a better topside spatial and temporal resolution of corresponding measurements so new Nano satellites missions as NanoMagSat should be very useful (Hulot et al., 2018, 2021). During the last decade, a number of studies have been devoted to validation of topside ionospheric N_e profile parameters by comparing the satellite-based Langmuir probes (LPs) observations with other ground and space-based techniques and model simulations (Lomidze et al., 2018; Catapano et al., 2022; McNamara et al., 2007; Pedatella et al., 2015; Rother et al., 2010; Yan et al., 2020; Liu et al., 2021; Park et al., 2016; Pignalberi et al., 2022).

In Lomidze et al. (2018) the authors calibrate and validate Swarm ionospheric N_e measured with LPs on the three Swarm satellites orbiting the Earth in circular, nearly polar orbits at ~500 km altitude using ISRs, low latitude ionosondes, and Constellation Observing System for Meteorology, Ionosphere, and Climate (COSMIC) satellites, covering all latitudes. The comparison results for plasma frequency for each Swarm satellite are consistent but that of the Swarm LPs systematically underestimate plasma frequency by about 10% (0.5–0.6 MHz). It has been found in Catapano et al. (2022) that plasma measurements are more accurate in dayside regions during high solar activity, while electron temperature measurements are more reliable during night side at middle and low latitudes during low solar activity. In Pignalberi et al. (2022) the Swarm B LP measurements were calibrated through Faceplate (FP) N_e observations from the same satellite. This can solve the N_e overestimation made by Swarm LP during night-time for low solar activity.

Studies on the ionospheric variations during geomagnetic storms using ground-based and in-situ observations from Swarm, CSES (China Seismo-Electromagnetic Satellite) and CHAMP (CHAllenging Minisatellite Payload) satellites have been realized (Pignalberi et al., 2016; Spogli et al., 2021; Astafyeva et al., 2022; Habarulema et al., 2020), next to studies that compare the models, as International Reference Ionosphere (IRI), with the satellite N_e observations (Bilitza et al., 2012; Klenzing et al., 2011, 2013). Pignalberi et al. (2016) showed that during the St. Patrick storm the IRI model cannot reproduce in-situ N_e observations but, as the authors underline, it should be expected considering that IRI is a monthly median model. Another interesting aspect that they found is that Swarm N_e is higher during the dusk terminator while the IRI N_e is higher during the dawn terminator. Comparisons of the IRI with N_e in-situ measurements of CHAMP, GRACE (Gravity Recovery and Climate Experiment) and C/NOFS (Communications/Navigation Outage Forecasting System) satellites during the deep solar minimum (2008–2009) have revealed significant overestimation of N_e by IRI at 400–500 km altitude, especially during daytime (Bilitza et al., 2012; Klenzing et al., 2011; Lühr and Xiong, 2010).

In this work, ionospheric N_e observations from satellite missions in a belt of 15° in latitude from 35°N to 50°N, and from 0° to 360° in longitude under different levels of solar activity have been used to define proper backgrounds for noon hours and night-time conditions and then characterize the mid-latitude ionospheric medium in terms of N_e abnormal variations from the backgrounds.

The electron densities from satellites are measured under different seasons and levels of solar and geomagnetic

activity. However, such observations are available at different times, heights, latitudes and longitudes and they cannot be directly used to create a background. Therefore, such observations need to be reduced to fixed times, heights and coordinates to be used. The only way to do this reduction is to use an empirical model like IRI (Bilitza et al., 2017) where temporal, spatial, and solar activity variations are given in the form of analytical expressions. The empirical climatologic IRI model is far from being perfect but today we do not have anything better. This was demonstrated during the inter-comparison of various models (empirical and physical, with and without data assimilation) made in the framework of the CEDAR project (Shim et al., 2011, 2012). The IRI model was shown to be one of the best at describing the F2-layer peak parameters N_mF2 and h_mF2 (maximum electron density and corresponding height, respectively) under various geophysical conditions. Moreover, a comparison with CHAMP in situ N_e observations in the topside has also shown that IRI manifests very good results (Shim et al., 2012). This justifies the use of the IRI model to reduce satellite N_e in situ observations.

Plasma data from the LPs onboard CHAMP (Reigber and Schwintzer, 1995) and Swarm (Friis-Christensen et al., 2008) satellites have been used in this work for the definition of the backgrounds, in which the IRI-2016 model (Bilitza et al., 2017) was used to reduce the satellites observations to reference times, heights and coordinates. The results have been compared to those obtained using a background made by the same version of the IRI model. The satellite missions, the IRI-2016 model, the background construction, and the ionospheric anomalies definition and classification in relation to the geomagnetic activity conditions are described in Section 2. In Section 3 some examples of the main results obtained for different solar activity conditions in the years 2004, 2009, 2016, and 2017, are presented in terms of the comparison of the satellites and IRI backgrounds behavior, as well as the classification of the anomalies in relation to the geomagnetic activity. The complete results under each condition can be found in the supplementary materials. Section 4 includes the discussion of the results, while in Section 5 the main conclusions are summarized.

2. Materials and methods

2.1. Satellite missions

2.1.1. CHAMP satellite

CHAMP was a German small satellite mission for geoscientific and atmospheric research and applications, managed by the German Research Centre for Geosciences (GFZ) (Reigber and Schwintzer, 1995). With its multifunctional and complementary payload elements, and its orbit characteristics, CHAMP generated highly precise gravity and magnetic field measurements simultaneously for the first time and over a 10-year period, as well as observations for atmospheric and ionospheric research and applications in weather prediction and space weather monitoring. The CHAMP satellite was launched on July 15, 2000, into an almost circular, near polar (87° of inclination) orbit with an initial altitude of 454 km and ended on September 19, 2010. 2004 and 2009 CHAMP N_e data have been used in this work. Such data have been acquired by the Langmuir Probe (LP) onboard the satellite and provided at a rate of 0.067 Hz (i.e., one sample every 15 s) in text file with "dat" extension as Level 2 data.

2.1.2. Swarm satellites

Swarm is a European Space Agency (ESA) mission launched on November 22, 2013, and still in orbit, consisting of a constellation of three identical satellites, called Alpha (A), Bravo (B) and Charlie (C), which provide precise simultaneous measurements of the magnetic field and ionospheric parameters over different regions of the Earth by means of a number of payloads onboard each satellite (Friis-Christensen et al., 2008). The satellites follow near-polar orbits at different altitudes: Swarm A and C fly in a lower orbit at around 460 km above the Earth's surface, while Swarm B is in the outer orbit (around 510 km). The state of the ionosphere is probed by a LP measuring the main plasma parameters, among which N_e is considered here for 2016 and 2017 years. Data used in this study are collected by the Swarm Langmuir Probe onboard each satellite and provided at a rate of 2 Hz as Level 1b data in common data format (CDF) files. The last release available at present, i.e., the 602, has been used and it includes important new calibrations performed on the plasma parameters, such as N_e and temperature (Lomidze et al., 2018).

2.2. International reference ionosphere (IRI) model

The International Reference Ionosphere (IRI) (Bilitza et al., 2022) is an international project sponsored by the Committee on Space Research (COSPAR) and the International Union of Radio Science (URSI), which provides one of the most used models of the complex ionospheric environment, recognized as the official standard for the Earth's ionosphere. The IRI is an empirical model for the primary ionospheric parameters, based on the long data record available from ground and space observations of the ionosphere. For a given location, time and date, the core model provides monthly averages of the N_e, electron temperature, ion temperature, and ion composition globally in the altitude range from 60 km to 2000 km. Being a data-based model, the IRI does not depend on the evolving theoretical understanding of the ionospheric processes, although its reliability depends on the spatial and temporal coverage provided by the underlying datasets. This means that the model is more reliable at mid-latitudes in the Northern hemisphere, thanks to the larger availability of data, given by a much denser network of ground stations. This is also the region investigated in this study. In the specific, to

compute the N_e at CHAMP or Swarm altitudes and at reference heights for the backgrounds definition (see section 2.3) the following options inside the IRI-2016 software package (Bilitza et al., 2017) have been used: (a) NeQuick model (Coïsson et al., 2006; Nava et al., 2008) for the topside ionosphere representation; (b) CCIR model for the N_e F2-peak (N_mF2); (c) Shubin (2015) model for the F2-peak height (h_mF2). All these options are the most recently recommended ones in most of the conditions and are the default options in the computer program.

2.3. Backgrounds definition

The goal of this work is to calculate a reference common N_e background at mid-latitude for a specific year, season, and local time, based on satellite data. For this purpose, the IRI-2016 model is used here not only for comparison, but also to adapt all the measurements, coming from different satellites at different heights, to a reference height for each condition. As shown in Fig. 1, the ionospheric region considered in this work extends in latitude from 35°N to 50°N, and from 0° to 360° in longitude.

A specific N_e background is here associated with each geographic cell with 3° latitude and 5° longitude size, within such a 15° latitudinal belt (i.e., 360 cells in total) for:

(i) each investigated year (2004, 2009, 2016, 2017);
(ii) each season, i.e., Winter (January, February, November, December), Equinox (March, April, September, October), and Summer (May, June, July, August);
(iii) noon hours (12 LT) and night-time (00 LT) conditions.

The selected altitudes for the calculation of each background, representing the reference satellites heights for the considered years, are: 375 km for 2004 (CHAMP); 320 km for 2009 (CHAMP); 475 km for 2016 and 2017 (Swarm). In Figs. 2 and 3, solar and geomagnetic activity levels during solar cycles 23 and 24 are shown, with the investigated years highlighted. The solar activity is represented by the progression of the sunspot number S_n (Clette and Lefèvre, 2016), while the geomagnetic activity by that of the planetary geomagnetic index A_p, which represents the daily mean of the 3-hourly geomagnetic index a_p (Matzka et al., 2021a, 2021b). Fig. 3 also shows the maximum level of geomagnetic activity achieved during each investigated year, as defined by the National Oceanic and Atmospheric Administration (NOAA) (http://www.swpc.noaa.gov/noaa-scales-explanation) on the base of the geomagnetic planetary K_p index, from which a_p is derived (Matzka et al., 2021a, 2021b). A maximum level of G2 (Moderate Storm) was achieved during 2009 and 2016, while G4 level (Severe Storm) was reached in 2004 and 2017.

Fig. 4 shows the local time of the CHAMP and Swarm satellites overflights over any location in the four investigated years; the data used for each season and for different times of the day (night-time or noon hours) have been highlighted with different colors. As CHAMP was a single satellite, it covered each day only two local times separated by 12 h, preceding 2.7 h per month. Grouping different months in our analysis, allows us to gather enough data for every season and time investigated. Taking into account that the behavior of the electron density is strictly related to seasonal variation of the ionosphere-thermosphere system, EUV total flux is comparable during Winter, Summer or Equinox months, and the thermospheric circulation does not change within a particular season. Swarm is a constellation of three satellites but as Alpha and Charlie fly side-by-side, their local times are very close, differently from Bravo. The precession of Alpha and Charlie is of 2.7 h per month, while Bravo precesses of 2.6 h per month.

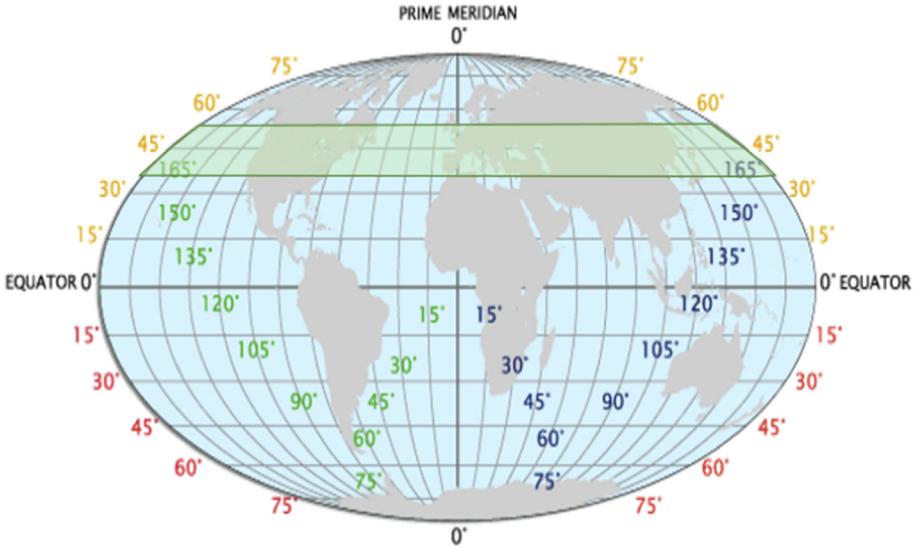

Fig. 1. Representation of the investigated region (green shaded box).

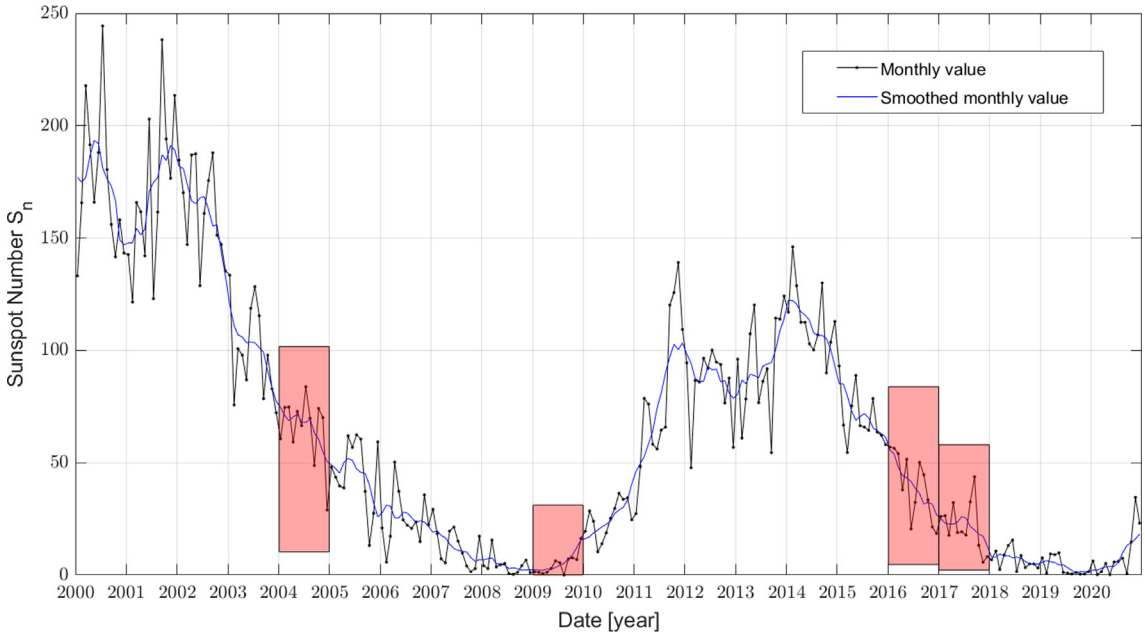

Fig. 2. Sunspot number progression for solar cycles 23 and 24, with the investigated years highlighted. Sunspot data from the World Data Center SILSO, Royal Observatory of Belgium, Brussels (https://www.sidc.be/silso/).

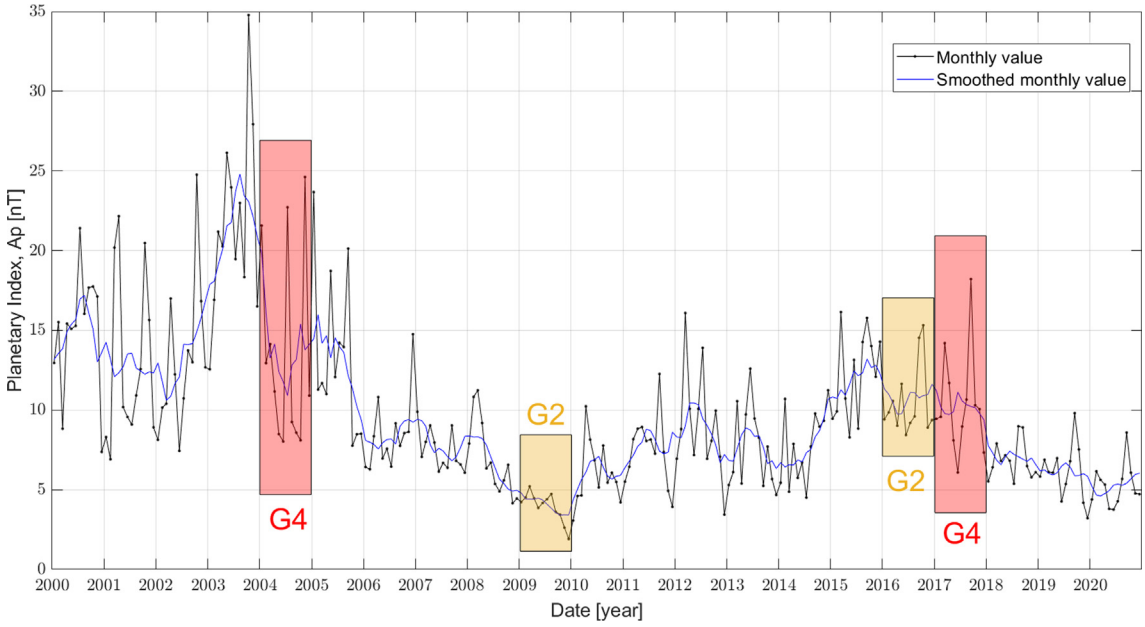

Fig. 3. Planetary geomagnetic index A_p progression for solar cycle 23 and 24; the maximum level of geomagnetic activity according to the NOAA scale (http://www.swpc.noaa.gov/noaa-scales-explanation) achieved during each investigated year is also indicated. A_p data from the World Data Center for Geomagnetism, Kyoto University, Kyoto (https://wdc.kugi.kyoto-u.ac.jp/).

The constellation assures a better coverage of the three seasons and the two selected local time hours to construct the backgrounds proposed in this study.

2.3.1. IRI backgrounds

The first type of used background consists in the mean, for each cell, for a specific condition (i.e., year, season, and local time) of the direct N_e output of IRI-2016 model, computed in the center of the cell at the reference altitude.

2.3.2. Satellite backgrounds

A second type of background is constructed using N_e data acquired by the satellites. This allows to reference all the measurements to common conditions and consequently strengthen and double-check the anomaly detection method. The N_e means for each condition are computed considering the satellite measurements in each specific cell with at least 10 samples inside from 11 LT to 13 LT for noon hours, and from 22 LT to 04 LT for

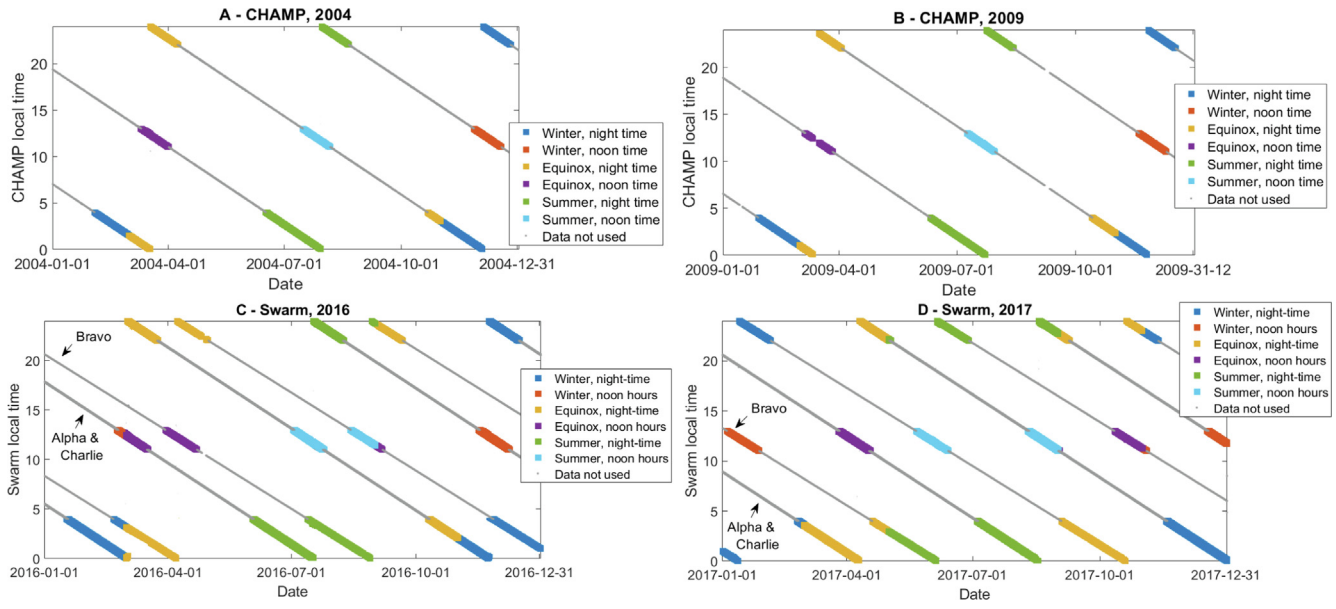

Fig. 4. Local time variation of the investigated satellites (A, B: CHAMP and C, D: Swarm) with underlined with different colors the samples used to construct the different backgrounds for each season and noon or nigh-time in 2004 (A), 2009 (B), 2016 (C) and 2017 (D). Swarm Alpha and Charlie flew in 2016 and 2017 with low longitudinal separation of 1.4° at the equator which produced a local time difference of about 6 min not distinguishable on this graph except for a slightly thicker line due to the superposition of the local time of the two satellites.

night-time. The time window for the background calculation at noon and night-time hours is different due to the differences in the characteristic lifetime of the ionospheric electrons under such conditions. Indeed, at mid-latitudes at noon hours the recombination characteristic time of O^+ is about 1–2 h, while during night-time it is around 10 h. This is due to the different height of the F2 layer, h_mF2, which is larger at night-time. Thus, during night the recombination process is less efficient, and the characteristic time is greater.

Before computing the means, each data sample is adjusted to the reference altitude and hour making use of the IRI-2016 model, as follows:

$$N_e(t_{ref}, h_{ref}) = N_{e,sat}(t_{sat}, h_{sat}) \cdot \frac{N_{e,IRI}(t_{ref}, h_{ref})}{N_{e,IRI}(t_{sat}, h_{sat})}, \quad (1)$$

where t_{ref} is equal to 12 LT or 00 LT depending on the day or night condition, h_{ref} depends on the year (see above), t_{sat} is in the time of satellite acquisition inside the interval 11–13 LT or 22–04 LT depending on the day or night condition, h_{sat} is the mean satellite altitude of the month. The monthly variations of satellite altitudes are negligible, while for the time used as input of the IRI model (t_{sat}) it has been chosen the UT o'clock time closer to the acquisition time.

2.4. Anomalies definition and classification

The deviation of the satellite Ne data with respect to the two computed backgrounds has been calculated inside time windows of 15 min. For Swarm satellites this implies that data potentially acquired by different satellites of the constellation within an interval of 15 min over the same cell, are grouped together to be compared with the background. The single satellite samples have been reported to their reference values by Eq. (1). Then, for each group of measurements over a specific cell the following quantity has been estimated:

$$\delta N_e = \frac{N_{e,sat} - N_{e,bkg}}{N_{e,bkg}}, \quad (2)$$

where $N_{e,sat}$ is the mean of all the samples acquired over the cell within 15 min, and $N_{e,bkg}$ is the corresponding IRI or satellite (CHAMP or Swarm) background. Then, positive and negative anomalies, depending on the sign of the deviation, have been defined if the mean of the grouped samples deviates more than 30% from the considered background. Each observed ionospheric anomaly has been classified in relation to the geomagnetic activity conditions, based on the values of the geomagnetic planetary index a_p

Table 1
Levels of geomagnetic activity according to the NOAA scale on the base of the a_p index (http://www.swpc.noaa.gov/noaa-scales-explanation), and the definition of the additional level G0+ based on the value of the AE index during the previous 6 h.

a_p (AE) nT	Geomagnetic Activity Level	Description
0–32 (≤100)	G0	Very Quiet
0–32 (>100)	G0+	Quiet
39–56	G1	Minor Storm
67–94	G2	Moderate Storm
111–154	G3	Strong Storm
179–300	G4	Severe Storm
400	G5	Extreme Storm

(Matzka et al., 2021a, 2021b) and the auroral electrojet index AE (World Data Center for Geomagnetism, Kyoto et al., 2015). In Table 1 are reported the level of geomagnetic activity in relationship with the changes in the a_p index, according to the NOAA scale (http://www.swpc.noaa.gov/noaa-scales-explanation). A further differentiation of the G0 level based on the AE index has been also defined in this work and reported in Table 1. Indeed, as the upsurges of auroral activity could produce perturbations of the mid-latitude ionospheric F2-layer (Kikuchi et al., 2000), the AE index values in the previous 6 h have been used to split the G0 level (i.e. the quietest) into 2 sub-levels, one with AE $\leq$ 100 nT (very quiet, so just G0) and the other with AE $>$ 100 nT (labeled with G0+).

3. Results

The methodology described above has been applied to CHAMP N_e data acquired during 2004 and 2009, and to Swarm satellites N_e measurements for the years 2016 and 2017. The complete results under each condition can be found in the supplementary materials. Here we present part of the main results, as a way of example. In particular, in the following section, we discuss for some selected cases:

- the distribution of the relative deviations between IRI and satellite backgrounds, along with the value of some statistical parameters such as Standard Deviation (SD), Mean Relative Deviation (MRD), and bias;
- the distribution of positive and negative anomalies against IRI and satellite backgrounds with respect to the geomagnetic activity levels.

For each cell and condition, the relative deviation between the two backgrounds has been computed as:

$$\delta N_{e,bkg}[\%] = \frac{N_{e,sat\_bkg} - N_{e,IRI\_bkg}}{N_{e,IRI\_bkg}}, \quad (3)$$

where N_{e,IRI_bkg} and N_{e,sat_bkg} represent the IRI and satellite N_e backgrounds, respectively. The vertical scale of the histograms has been selected with a common value for each group of analysis to easily and quickly compare the obtained results. In particular, 140 and 170 cells have been chosen for the relative deviation between IRI background and CHAMP and Swarm ones, respectively.

3.1. Analysis of 2004 and 2009 CHAMP data

The above-described procedure was applied to CHAMP data acquired during the years 2004 and 2009. It is worth noting that these two years correspond to different solar activity, since 2004 represents mid solar activity after the maximum of the 23rd solar cycle, while 2009 corresponds to a deep minimum in the solar activity.

3.1.1. Comparison between the IRI and CHAMP backgrounds for 2004 and 2009

The $\delta N_{e,bkg}[\%]$ distributions obtained for the years 2004 and 2009, along with the corresponding SD and MRD, have been calculated for each season and night-time or noon hours condition. As can be noticed in the examples reported in Fig. 5, the IRI background tends to reach values greater than those of the CHAMP background.

3.1.2. Anomalies with respect to the IRI background for 2004 and 2009

As described in Section 2.4, the N_e variations greater than 30% from a reference background have been considered as anomalous. The anomalies observed in 2004 and 2009 with respect to the IRI background are further investigated in this subsection classifying them according to the different geomagnetic activity levels and seasons, for both night-time and noon hours. As an example, we show in Fig. 6, the distribution of positive (red bars) and negative (blue bars) anomalies for Winter 2004 observed during night-time (panel (a)), together with the distribution of

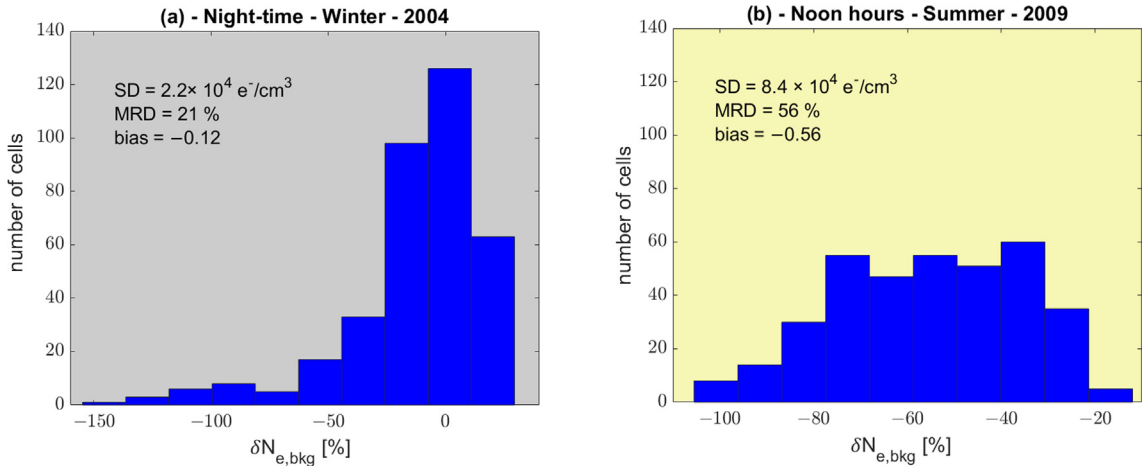

Fig. 5. Distribution of the relative deviation $\delta N_{e,bkg}[\%]$ between CHAMP and IRI backgrounds: (a) Night-time, Winter 2004; (b) Noon hours, Summer 2009. The values of the Standard Deviation (SD), Mean Relative Deviation (MRD) and bias are also provided.

the anomalies for Summer 2009 occurred during noon hours (panel (b)). It can be noticed that in almost all the cases a larger number of negative anomalies have been revealed with respect to the positive ones. The abundance of negative anomalies suggests a systematic overestimation of electron density by the IRI model.

3.1.3. Anomalies with respect to the CHAMP background in 2004 and 2009

The same method for the detection of the anomalies in the electron density has been applied considering the background obtained using CHAMP N_e data. As can be seen from Fig. 7, in this case there is a better balance between negative and positive anomalies.

3.2. Analysis of 2016 and 2017 Swarm data

Since CHAMP satellite mission has been decommissioned in 2010, data from the Swarm satellite constellation have been used to characterize the mid-latitude topside ionospheric N_e for 2016 and 2017. The results are presented in the following subsections. Similarly to 2004, 2016 and 2017 represent mid solar activity after the maximum of the 24th solar activity cycle, although such a cycle was remarkably weaker than the previous one.

3.2.1. Comparison between the IRI and Swarm backgrounds for 2016 and 2017

The relative differences between Swarm N_e and IRI model backgrounds during 2016 and 2017 for night-time and noon hours respectively, along with the corresponding values of SD, MRD and bias, are calculated. As can be seen in the examples shown in Fig. 8, for both years an overestimation of the IRI background is confirmed during noon hours, while an underestimation is seen during night-time.

3.2.2. Anomalies with respect to the IRI background in 2016 and 2017

Night-time and noon hours anomalies computed considering the IRI background for 2016 and 2017 are presented and classified for geomagnetic activity and season. As can be seen in the examples of Fig. 9, during night-time hours of Winter and Summer, a larger number of positive anoma-

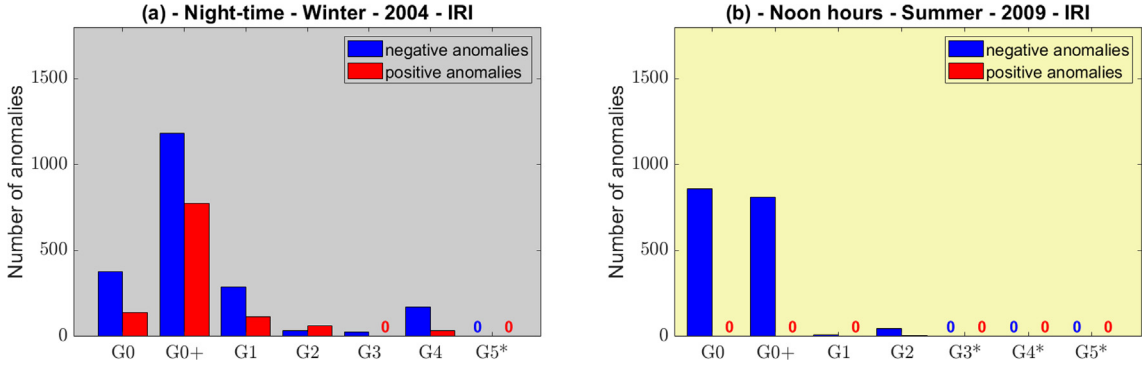

Fig. 6. Distribution of the positive (in red) and negative (in blue) anomalies with respect to the IRI background through the different geomagnetic activity levels: (a) Night-time, Winter 2004; (b) Noon hours, Summer 2009. In case no negative or positive anomalies are identified, a blue or red "0" is reported respectively on the corresponding level. The asterisk "*" indicates that such a level was not reached during the corresponding hours of the specific season.

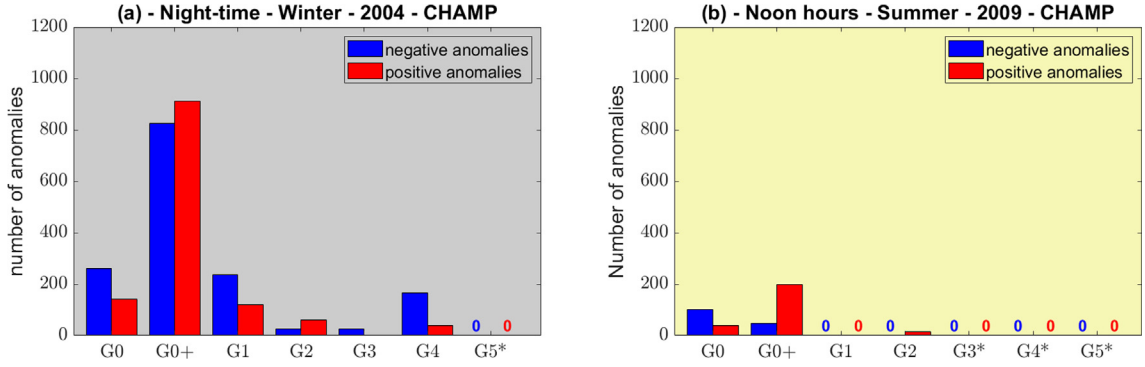

Fig. 7. Distribution of the positive (in red) and negative (in blue) anomalies with respect to the CHAMP background through the different geomagnetic activity levels: (a) Night-time, Winter 2004; (b) Noon hours, Summer 2009. The "0" and "*" symbols mark the absence of anomalies or days in the corresponding level, respectively.

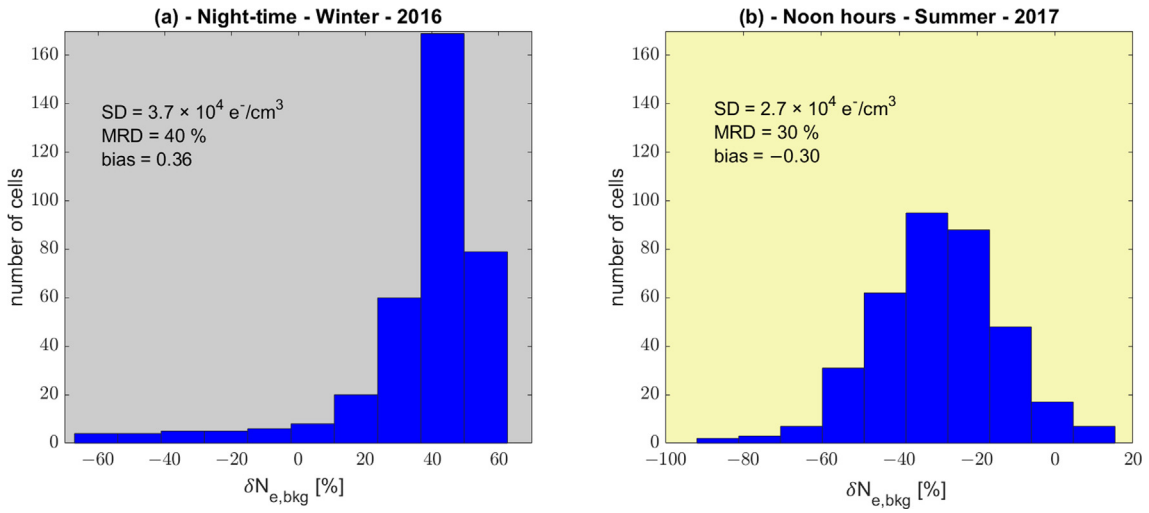

Fig. 8. Distribution of the relative deviation $\delta N_{e,bkg}[\%]$ between Swarm and IRI backgrounds during: (a) Night-time, Winter 2016; (b) Noon hours, Summer 2017. The values of the Standard Deviation (SD), Mean Relative Deviation (MRD) and bias are also provided.

lies with respect to negative ones confirms the observed underestimation of the IRI model. Conversely, the largely predominant number of negative anomalies during noon hours is a clear indication of the overestimation introduced by the IRI model in such a condition during all the seasons.

3.2.3. Anomalies with respect to the Swarm background in 2016 and 2017

The anomalies observed when Swarm satellite background for 2016 and 2017 is considered, have been classified in relation to the geomagnetic activity. As it is shown in the examples of Fig. 10, the negative anomalies are greater in number during both night-time and noon hours under almost all levels of geomagnetic activity and seasons. An exception is found for noon hours in 2016, where positive anomalies overcome negative ones (see Fig. S18 of the supplementary materials).

4. Discussion

In this work we studied plasma data from CHAMP satellite for 2004 (medium solar activity) and 2009 (solar minimum), and from Swarm satellites for 2016 and 2017 (mid-low solar activity during the descending phase of the solar cycle).

The study of the ionospheric electron density variations needs the definition of a reliable background suitable for the investigated conditions. However, the electron density data coming from satellite measurements are not sufficient to allow the construction of a solid N_e background for every hour and month of the years here analyzed. To overcome this problem, we grouped N_e data in seasons, taking in mind that the behavior of the electron density is strictly related to the seasonal variation of the ionosphere-thermosphere system. Indeed, the EUV total flux is similar in the months that belong to Winter or Summer or Equinox, and the thermospheric circulation is the same within the same season. This permits us to group the electron density data observed in the different months in order to construct a solid and stable background. For the same reason, it has been necessary to group the hours within different time windows for noon and night-time hours due to the different characteristic time of recombination of O^+.

The comparison between the backgrounds calculated with CHAMP means and the IRI-2016 model for 2004 and 2009, gives the following results:

- During night-time a better agreement between the two backgrounds, highlighted also by the values of the statistic parameters, can be noticed;
- During noon hours it is more evident the overestimation of the N_e introduced by the IRI model.

The overestimation of the IRI model is confirmed also by the great number of noon hours negative anomalies using IRI as background. This is evident in particular in 2009, a year of a very deep solar minimum, where we can see only negative anomalies for all the seasons in contradiction to what is expected. Indeed, it is well known that negative storms generally occur during night-time when the thermospheric wind flows equatorward, and under an increase of geomagnetic activity (Prölss, 1995). Our results are in line with those presented by Lühr and Xiong (2010) and Bilitza and Xiong (2021), who pointed out an IRI overestimation during the deep solar minimum during the years 2008–2009.

It is noteworthy that using the background computed using CHAMP N_e data, a higher number of negative anomalies with respect to the positive ones has been found during noon hours in Winter season under magnetically very quiet conditions (see Fig. S12(a) of the supplementary materials). This could be due to the effect of the Sudden Stratospheric Warmings that occurred in January 2009, which contributed to increase the number of negative iono-

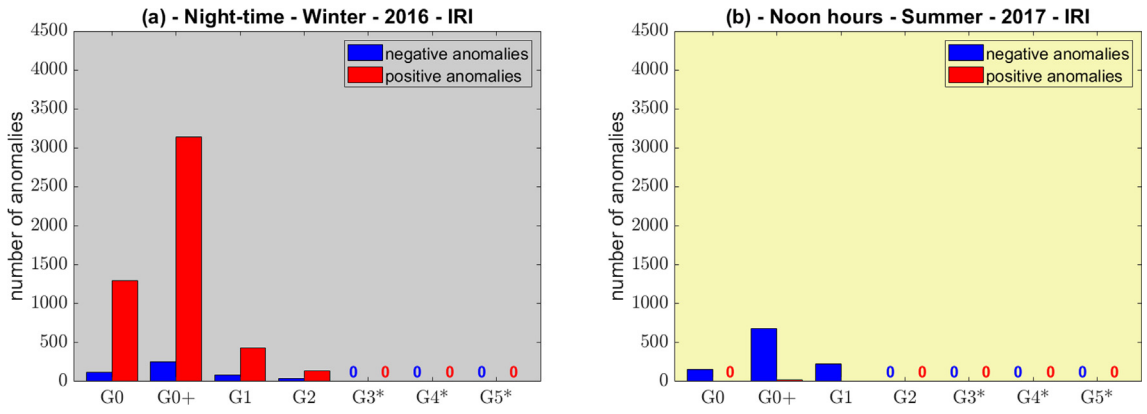

Fig. 9. Distribution of the positive (in red) and negative (in blue) anomalies with respect to the IRI background through the different geomagnetic activity levels: (a) Night-time, Winter 2016; (b) Noon hours, Summer 2017. The "0" and "*" symbols mark the absence of anomalies or days in the corresponding level, respectively.

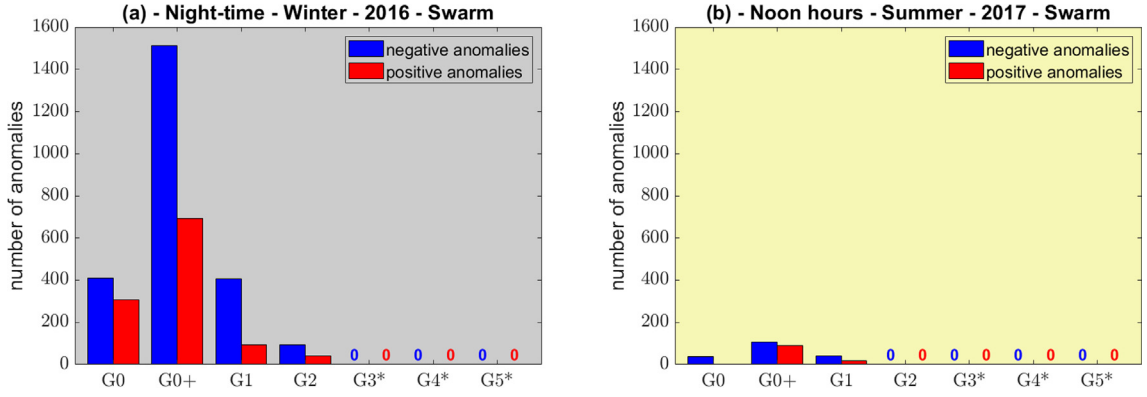

Fig. 10. Distribution of the positive (in red) and negative (in blue) anomalies with respect to the Swarm background through the different geomagnetic activity levels: (a) Night-time, Winter 2016; (b) Noon hours, Summer 2017. The "0" and "*" symbols mark the absence of anomalies or days in the corresponding level, respectively.

spheric anomalies (Mikhailov and Perrone, 2023; Mikhailov et al., 2021).

The comparison between the backgrounds calculated with Swarm means and the IRI-2016 model for 2016 and 2017, gives the following results:

- During night-time a better agreement between the two backgrounds is confirmed for 2016, particularly for Equinox season (Fig. S13(b) of the supplementary materials);
- An underestimation of IRI with respect to Swarm background occurs for both years in night-time conditions;
- During noon hours the evident overestimation of the N_e introduced by the IRI model is also confirmed.

These results confirm what has been found by Singh et al. (2021) and Smirnov et al. (2021). Comparing the Swarm N_e data with IRI (Singh et al., 2021) in quiet periods, they found that N_e from Swarm A and Swarm B is higher than IRI-2016 estimations during night-time, while it appears to be lower during daytime. The same result has been evidenced by Pignalberi et al. (2016), who found that Swarm LP N_e observations are characterized by an overestimation during night-time hours that is overcompensated by an underestimation during daytime hours. However, it should be taken into account that plasma measurements are more accurate in dayside regions during high solar activity (Catapano et al., 2022).

Finally, it should be noted that the analysis of 2004 plasma data, when G4 geomagnetic activity level was reached, suggests that IRI could be used as a background for high levels of geomagnetic activity, since, in such conditions, strong anomalies can be detected also against a biased background. However, for ionospheric anomalies that occur during quiet geomagnetic conditions, i.e., the so-called Q-disturbances (Perrone et al., 2020), it is discouraged to use IRI as a background. In this respect, Fig. 11 shows the yearly averaged MRD behavior with solar activity, as represented by the yearly sunspot number. As can be seen, a better agreement between satellites and IRI backgrounds as solar activity increases is demonstrated, confirming better perfor-

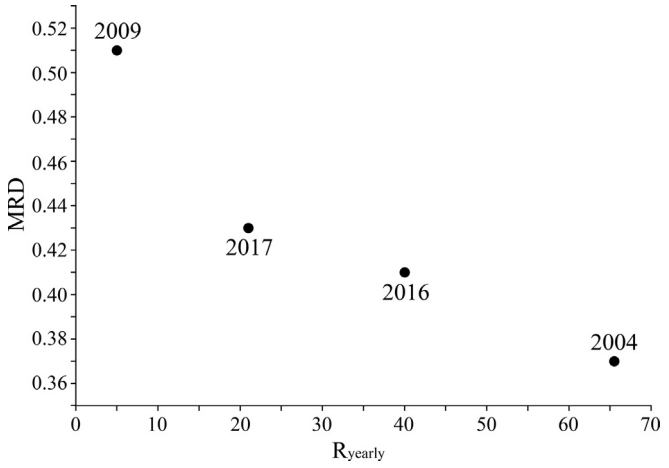

Fig. 11. Yearly averaged MRD behavior with solar activity. R_{yearly} represents the yearly sunspot number. Sunspot data from the World Data Center SILSO, Royal Observatory of Belgium, Brussels (https://www.sidc.be/silso/).

mances of the IRI model for 2004 with respect to the other investigated years.

This could explain why in 2004 the number of G4-classified anomalies with respect to IRI and satellite backgrounds is in a better agreement than the number of the same kind of anomalies observed in 2017, when the differences between the two backgrounds are more pronounced. This is highlighted in Fig. 12.

5. Conclusions

In conclusion:

1. The electron density backgrounds defined in this work, on the basis of in-situ N_e measurements from satellites probing the topside ionosphere at mid-latitudes, proved to be suitable for ionospheric anomaly detection close to local midday and midnight hours, in every season and different solar and geomagnetic conditions;
2. The comparison of the results obtained using satellite and IRI model-based backgrounds highlighted a general disagreement between the two kinds of backgrounds, particularly during noon hours, when IRI background overestimates satellite N_e measurements in all conditions;
3. The general disagreement between IRI and satellites backgrounds decreases as solar activity increases (although the highest levels of solar activity are not investigated in this study); this suggests that IRI background could be used for high levels of geomagnetic activity under high solar activity conditions.
4. The IRI model has been improved with a solar activity dependent correction for the topside N_e (Bilitza and Xiong, 2021) so there is the future possibility to test the use of the new IRI-2020 version (Bilitza et al., 2022) as a background also for periods with solar minimum activity.

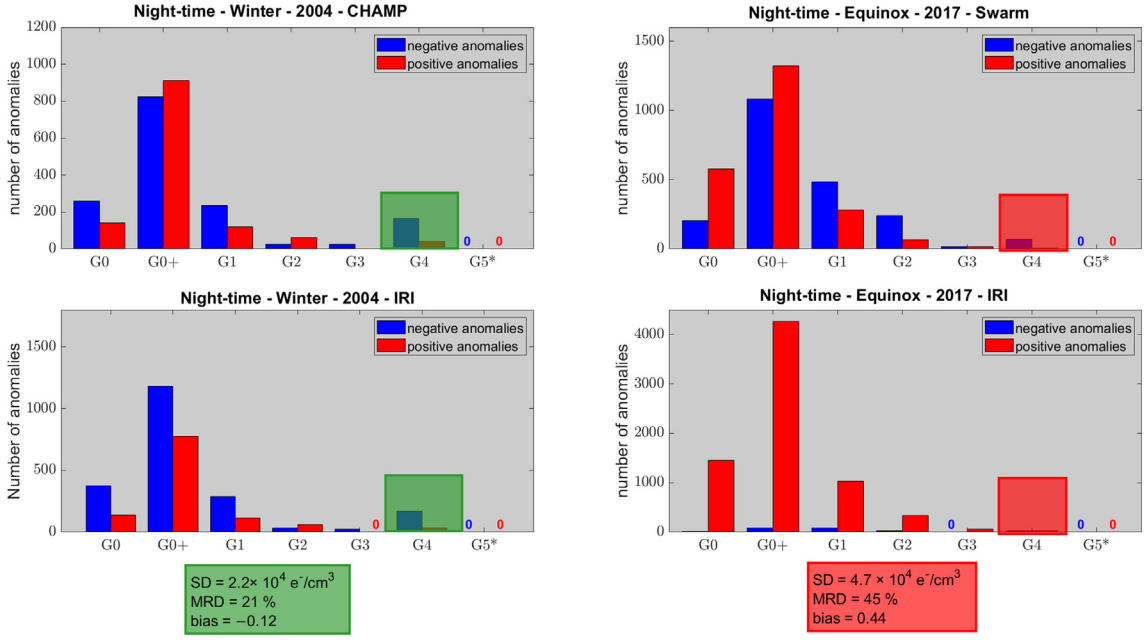

Fig. 12. Anomalies respect to satellites (top) and IRI (bottom) backgrounds for 2004 Winter 0 LT (left) and 2017 Equinox 0 LT (right), along with the corresponding statistical parameters characterizing the relative deviations between the two kinds of backgrounds (center); G4-classified anomalies and statistical parameters are highlighted with green (2004) and red (2017) squares to underline the better agreement between the two kinds of backgrounds obtained in 2004 with respect to 2017.

Funding

This research was funded by the European Space Agency (ESA), grant number 4000113862/15/NL/MP, extension (e-SAFE) of the project SAFE (SwArm For Earthquake study) and by the Italian Space Agency (ASI), grant number 2020-32-H.0 of the Limadou Scienza + project. The Open Access publishing charges have been covered by the Italian National Institute of Geophysics and Volcanology (INGV).

Declaration of Competing Interest

The authors declare that they have no known competing financial interests or personal relationships that could have appeared to influence the work reported in this paper.

Acknowledgement

This work was undertaken in the framework of the extension (e-SAFE) of the ESA-funded project SAFE (Swarm for Earthquake study), and under the Limadou Scienza + project funded by the ASI. S.A.C. acknowledges Juan de la Cierva-Incorporación programme. D.M. acknowledges the National Natural ScienceFoundation of China (grant 41974084). The authors also thank all the providers of the data used in this work, and the IRI community.

Appendix A. Supplementary material

Supplementary data to this article can be found online at https://doi.org/10.1016/j.asr.2023.05.029.

References

Astafyeva, E., Yasyukevich, Y.V., Maletckii, B., Oinats, A., Vesnin, A., Yasyukevich, A.S., et al., 2022. Ionospheric disturbances and irregularities during the 25–26 August 2018 geomagnetic storm e2021JA029843. J. Geophys. Res.: Space Phys. 127. https://doi.org/10.1029/2021JA029843.

Bilitza, D., Brown, S.A., Wang, M.Y., Souza, J.R., Roddy, P.A., 2012. Measurements and IRI model predictions during the recent solar minimum. J. Atmos. Solar-Terr. Phys. 86, 99–106. https://doi.org/10.1016/j.jastp.2012.06.010.

Bilitza, D., Altadill, D., Truhlik, V., Shubin, V., Galkin, I., Reinisch, B., Huang, X., 2017. International Reference Ionosphere 2016: From ionospheric climate to real-time weather predictions. Space Weather 15, 418–429. https://doi.org/10.1002/2016SW001593.

Bilitza, D., Pezzopane, M., Truhlik, V., Altadill, D., Reinisch, B.W., Pignalberi, A., 2022. The International Reference Ionosphere model: A review and description of an ionospheric benchmark e2022RG000792. Revi. Geophys. 60. https://doi.org/10.1029/2022RG000792.

Bilitza, D., Xiong, C., 2021. A solar activity correction term for the IRI topside electron density model. Adv. Space Res. 68 (5), 2124–2137. https://doi.org/10.1016/j.asr.2020.11.012.

Catapano, F., Buchert, S., Qamili, E., Nilsson, T., Bouffard, J., Siemes, C., Coco, I., D'Amicis, R., Tøffner-Clausen, L., Trenchi, L., Holmdahl Olsen, P.E., Stromme, A., 2022. Swarm Langmuir probes' data quality validation and future improvements. Geosci. Instrum. Method. Data Syst. 11, 149–162. https://doi.org/10.5194/gi-11-149-2022.

Clette, F., Lefèvre, L., 2016. The new sunspot number: assembling all corrections. Sol Phys 291, 2629–2651. https://doi.org/10.1007/s11207-016-1014-y.

Coïsson, P., Radicella, S.M., Leitinger, R., Nava, B., 2006. Topside electron density in IRI and NeQuick: Features and limitations. Adv. Space Res. 37 (5), 937–942. https://doi.org/10.1016/j.asr.2005.09.015.

Fiori, R.A.D., Kumar, V.V., Boteler, D.H., Terkildsen, M.B., 2022. Occurrence rate and duration of space weather impacts on high-frequency radio communication used by aviation. J. Space Weather Space Clim. 12 (21), 607. https://doi.org/10.1051/swsc/2022017.

Frank-Kamenetsky, A., Troshichev, O., 2012. A relationship between the auroral absorption and the magnetic activity in the polar cap. J. Atmos. Sol. Terr. Phys. 77, 40–45.

Friis-Christensen, E., Lühr, H., Knudsen, D., Haagmans, R., 2008. Swarm—An Earth observation mission investigating geospace. Adv. in Space Res. 41 (1), 210–216.

Fuller-Rowell, T.J., Codrescu, M.V., Moffett, R.J., Quegan, S., 1994. Response of the thermosphere and ionosphere to geomagnetic storm. J Geophys Res 99, 3893–3914. https://doi.org/10.1029/93JA02015.

Habarulema, J.B., Katamzi-Joseph, Z.T., Burešová, D., Nndanganeni, R., Matamba, T., Tshisaphun go, M., et al., 2020. Ionospheric response at conjugate locations during the 7–8 September 2017 geomagnetic storm over the Europe-African longitude sector e2020JA028307. J. Geophys. Res.: Space Phys. 125. https://doi.org/10.1029/2020JA028307.

Hargreaves, J.K., Birch, M.J., Bromage, B.J.I., 2007. D- and E-region effects in the auroral zone during a moderately active 24-h period in July 2005. Ann. Geophys. 25, 1837–1849.

Hulot, G., Léger, J.-M., Clausen, L. B. N., Deconinck, F., Coïsson, P., Vigneron, P., Alken, P., Chulliat, A., Finlay, C. C., Grayver, A., Kuvschinov, A., Olsen, N., Thébault, E., Jager, T., Bertrand, F., Häfner, T., 2021. NanoMagSat, a 16U nanosatellite constellation high-precision magnetic project to initiate permanent low-cost monitoring of the Earth's magnetic field and ionospheric environment, EGU General Assembly 2021, online, 19–30 Apr 2021, EGU21-14660, https://doi.org/10.5194/egusphere-egu21-14660.

Hulot, G., Léger, J., Vigneron, P., Jager, T., Bertrand, F.O., Coïsson, P., Deram, P., Boness, A., Tomasini, L., Faure, B., 2018. Nanosatellite high-precision magnetic missions enabled by advances in a stand-alone scalar/vector absolute magnetometer. In: 2018 IEEE International Geoscience and Remote Sensing Symposium, pp. 6320–6323. https://doi.org/10.1109/IGARSS.2018.8517754.

Kauristie, K., Andries, J., Beck, P., Berdermann, J., Berghmans, D., Cesaroni, C., De Donder, E., de Patoul, J., Dierckxsens, M., Doornbos, E., et al., 2021. Space Weather Services for Civil 603 Aviation—Challenges and Solutions. Remote Sens. (Basel) 13, 3685. https://doi.org/10.3390/604 rs13183685. 605.

Kikuchi, T., Lühr, H., Schlegel, K., Tachihara, H., Shinohara, M., Kitamura, T.-I., 2000. Penetration of auroral electric fields to the equator during a substorm. J. Geophys. Res. 105 (A10), 23251–23261.

Klenzing, J., Simões, F., Ivanov, S., Heelis, R.A., Bilitza, D., Pfaff, R., Rowland, D., 2011. Topside equatorial ionospheric density and composition during and after extreme solar minimum. J. Geophys. Res. 116, A12330. https://doi.org/10.1029/2011JA017213.

Klenzing, J., Simões, F., Ivanov, S., Bilitza, D., Heelis, R.A., Rowland, D., 2013. Performance of the IRI-2007 model for equatorial topside ion density in the African sector for low and extremely low solar activity. Adv. Space Res. 52 (10), 1780–1790. https://doi.org/10.1016/j.asr.2012.09.030.

Liu, J., Guan, Y., Zhang, X., Shen, X., 2021. The data comparison of electron density between CSES and DEMETER satellite, swarm constellation and IRI model. Earth Space Sci. 8, 2. https://doi.org/10.1029/2020EA001475, e2020EA001475.

Lomidze, L., Knudsen, D.J., Burchill, J., Kouznetsov, A., Buchert, S.C., 2018. Calibration and validation of Swarm plasma densities and

electron temperatures using ground-based radars and satellite radio occultation measurements. Radio Sci. 53, 15–36. https://doi.org/10.1002/2017RS006415.

Lühr, H., Xiong, C., 2010. IRI-2007 model overestimates electron density during the 23/24 solar minimum. Geophys. Res. Lett. 37, L23101. https://doi.org/10.1029/2010GL045430.

Matzka, J., Bronkalla, O., Tornow, K., Elger, K., Stolle, C., 2021a. Geomagnetic Kp index. V. 1.0, GFZ Data Services, https://doi.org/10.5880/Kp.0001.

Matzka, J., Stolle, C., Yamazaki, Y., Bronkalla, O., Morschhauser, A., 2021b. The geomagnetic Kp index and derived indices of geomagnetic activity e2020SW002641. Space Weather 19. https://doi.org/10.1029/2020SW002641.

McNamara, L.F., Cooke, D.L., Valladares, C.E., Reinisch, B.W., 2007. Comparison of CHAMP and digisonde plasma frequencies at Jicamarca. Peru, Radio Sci. 42, 1–14.

Mikhailov, A.V., Perrone, L., 2023. Whether sudden stratospheric warming effects are seen in the mid-latitude thermosphere of the opposite hemisphere? e2023JA031285. J. Geophys. Res.: Space Phys. 128. https://doi.org/10.1029/2023JA031285.

Mikhailov, A.V., Perrone, L., Nusinov, A.A., 2021. Mid-latitude daytime F2-layer disturbance mechanism under extremely low solar and geomagnetic activity in 2008–2009. Remote Sens. 13, 1514. https://doi.org/10.3390/rs13081514.

Nava, B., Coïsson, P., Radicella, S.M., 2008. A new version of the NeQuick ionosphere electron density model. J. Atmos. Sol. Terr. Phys. 70 (15), 1856–1862. https://doi.org/10.1016/j.jastp.2008.01.015.

Park, J., Kil, H., Stolle, C., Lühr, H., Coley, W.R., Coster, A., Kwak, Y.-S., 2016. Daytime midlatitude plasma depletions observed by Swarm: topside signatures of the rocket exhaust. Geophys. Res. Lett. 43, 1802–1809. https://doi.org/10.1002/2016GL067810.

Pedatella, N.M., Yue, X., Schreiner, W.S., 2015. Comparison between GPS radio occultation electron densities and in situ satellite observations. Radio Sci. 50, 518–525. https://doi.org/10.1002/2015RS005677.

Perrone, L., Mikhailov, A., Nusinov, A., 2020. Daytime mid-latitude F-2-layer Q-disturbances: A formation mechanism. Sci. Rep. 10, 9997. https://doi.org/10.1038/s41598-020-66134-2.

Pignalberi, A., Pezzopane, M., Tozzi, R., et al., 2016. Comparison between IRI and preliminary Swarm Langmuir probe measurements during the St. Patrick storm period. Earth Planet Sp 68, 93. https://doi.org/10.1186/s40623-016-0466-5.

Pignalberi, A., Pezzopane, M., Coco, I., Piersanti, M., Giannattasio, F., De Michelis, P., Tozzi, R., Consolini, G., 2022. Inter-calibration and statistical validation of topside ionosphere electron density observations made by CSES-01 mission. Remote Sens. 14, 4679. https://doi.org/10.3390/rs14184679.

Prölss, G.W., 1991. Thermosphere-ionosphere coupling during disturbed conditions. J. Geomag. Geoelectr. 43 (Suppl), 537–549. https://doi.org/10.5636/jgg.43.Supplement1_537.

Prölss, G.W., 1995 Ionospheric F-region storms. In: Handbook of Atmospheric Electrodynamics, 1st ed.; H., V., Ed.; CRC Press, Boca Raton, FL, USA; Chapter 8, pp. 195–248. https://doi.org/10.1201/9780203713297.

Reigber, C., Schwintzer, P., 1995. A Challenging Microsatellite Payload for Geophysical Research and Application. Small Satellites for Remote Sensing, Space Congress 1995, Bremen, Germany, May 24–25, pp. 83–89.

Rother, M., Schlegel, K., Lühr, H., Cooke, D., 2010. Validation of CHAMP electron temperature measurements by incoherent scatter radar data. Radio Sci. 45, RS6020. https://doi.org/10.1029/2010RS004445.

Shim, J.S. et al., 2011. CEDAR Electrodynamics Thermosphere Ionosphere (ETI) Challenge for systematic assessment of ionosphere/thermosphere models: NmF2, and hmF2, and vertical drift using ground-based observations. Space Weather 9, S12003. https://doi.org/10.1029/2011SW000727.

Shim, J.S. et al., 2012. CEDAR Electrodynamics Thermosphere Ionosphere (ETI) Challenge for systematic assessment of ionosphere/thermosphere models: Electron density, neutral density, NmF2, and hmF2 using space based observations. Space Weather 10, S10004. https://doi.org/10.1029/2012SW000851.

Shubin, V.N., 2015. Global median model of the F2-layer peak height based on ionospheric radio-occultation and ground based Digisonde observations. Adv. Space Res. 56 (5), 916–928. https://doi.org/10.1016/j.asr.2015.05.029.

Singh, A., Maltseva, O., Panda, S., 2021. Comparison between Swarm measured and IRI-2016, IRI-Plas 2017 modeled electron density over low and mid latitude region. Acta Astronaut. 189, 476–482. https://doi.org/10.1016/j.actaastro.2021.09.017.

Smirnov, A., Shprits, Y., Zhelavskaya, I., Lühr, H., Xiong, C., Goss, A., Prol, F.S., Schmidt, M., Hoque, M., Pedatella, N., et al., 2021. Intercalibration of the plasma density measurements in Earth's topside ionosphere. J. Geophys. Res. Space Phys. 126, e2021JA029334.

Spogli, L., Sabbagh, D., Regi, M., Cesaroni, C., Perrone, L., Alfonsi, L., et al., 2021. Ionospheric response over Brazil to the August 2018 geomagnetic storm as probed by CSES-01 and Swarm satellites and by local ground-based observations e2020JA028368. J. Geophys. Res.: Space Phys. 126. https://doi.org/10.1029/2020JA028368.

World Data Center for Geomagnetism, Kyoto, Nose M., Iyemori T., Sugiura M., Kamei, T., 2015. Geomagnetic AE index, https://doi.org/10.17593/15031-54800.

Yan, R., Zhima, Z., Xiong, C., Shen, X., Huang, J., Guan, Y., Zhu, X., Liu, C., 2020. Comparison of electron density and temperature from the CSES satellite with other space-borne and ground-based observations. J. Geophys. Res.: Space Phys. 125, 10. https://doi.org/10.1029/2019JA027747.